Available online at www.sciencedirect.com

SciVerse ScienceDirect

Ceramics International 39 (2013) 6087–6098

CERAMICS INTERNATIONAL

www.elsevier.com/locate/ceramint

Approach of phase transformations and densification in nanostructured and (Bi_2O_3, ZnO, TiO_2) doped silica ceramics

Lucie Nguyen[a], Alexandre Maître[a,*], Martine Lejeune[a], Chrystelle Dossou-Yovo[b], Rémi Noguéra[b], Renaud Podor[c]

[a]*Centre Européen de la Céramique, SPCTS, UMR CNRS 7315, 12 rue Atlantis, F-87068 Limoges, France*
[b]*Ceradrop, 32 Rue Soyouz, F-87068 Limoges, France*
[c]*ICSM-UMR 5257 CEA-CNRS-UM2-ENSCM, Site de Marcoule, Bât. 426, BP 17171, F-30207 Bagnols sur Cèze, France*

Received 12 December 2012; received in revised form 8 January 2013; accepted 9 January 2013
Available online 17 January 2013

Abstract

The low temperature sintering of silica is studied under the influence of sintering aids and nanosized powders using X-Ray Diffractometry (XRD) and high-temperature environmental scanning electron microscopy analyses (HT-ESEM). Two particular aids were chosen to conduct this study, $[Bi_2O_3–ZnO]_{eutectic}$ and titania. We report a lowering of the crystallization temperature when the former compound is introduced in the silica while a raise is observed when the latter is used. Moreover, the amorphous silica crystallization into cristobalite inhibits drastically the kinetics of densification of silica-based materials.

Keywords: A. Sintering; B. Electron Microscopy; B. Microstructure-final; D. SiO_2

1. Introduction

Silica (SiO_2) is a promising ceramic material by its numerous applications such as optical communication fibers, quartz oscillators, insulating films and dielectric materials. For microelectronic applications, silica could be coupled with other materials, and in particular to cheap conductive materials such as silver [1]. This combination of a dielectric material and of a conductive material allows the fabrication of multi-components as transistors.

It is well known that the sintering temperature of silica is higher than its glass transition temperature ($Tg \approx 1200\ ^\circ C$ [2,3]) whereas the melting point of silver remains lower (*i.e.* 961 °C). This wide discrepancy between the Tg and T_M values, the thermal expansion coefficients (*i.e.* $5 \times 10^{-7}\ ^\circ C^{-1}$ for silica and $2 \times 10^{-5}\ ^\circ C^{-1}$ for silver), and consequently, their respective sintering temperatures, promotes the appearance of residual stresses at the metal/SiO_2 interface.

To overcome the residual swelling effect of the ceramic and metal layers and the microcracks at the metal/ceramic layers interface, it is usually required to lower the sintering temperature of the silica-based materials to make it in agreement with that of conductive material. Two ways could be investigated in order to reach this target: firstly, the use of nanosized starting powders, and secondly, the introduction of sintering additives.

The first path was studied by Wu et al. [4] who analyzed the influence of the mean particle size of silica nanopowders on their sintering behavior. In particular, they showed that the use of finer particles would lead to higher reactivity and lower sintering temperature. Thus, full dense silica sintered bodies were obtained after a soaking treatment at 900 °C during 24 h. In the latter case, the mean diameter of nanoparticles ranges between 7 and 10 nm. Besides, Popma [5] showed that to reach full dense bodies from silica sol–gel precursors (the size of colloids is around 25 nm) a sintering at 1100 °C of 3 h is required. Moreover,

*Corresponding author: Tel.: +33 5 87 50 23 48; fax: +33 5 87 50 23 07.
E-mail address: alexandre.maitre@unilim.fr (A. Maître).

0272-8842/$ - see front matter © 2013 Elsevier Ltd and Techna Group S.r.l. All rights reserved.
http://dx.doi.org/10.1016/j.ceramint.2013.01.026

the dwell time at the same temperature seems to be dependent on the colloids size: 20 h for colloids of 50 nm, 40 h for a mean diameter of 90 nm.

The second way relies on the use of sintering aids which could break the Si–O–Si bridges and could promote either (substitutional or interstitial) solid solutions or the appearance of a liquid phase [2]. In the latter case, the densification kinetic of silica-based ceramics could be enhanced by decreasing the crystallization rate or by improving either the rearrangement of particles or the mass transfer by diffusion within the liquid phase. Among the sintering additives reported in the literature, B_2O_3 [6], B_2O_3–CaO [7,8], P_2O_5–ZnO [9] seem to be used even if their role on the densification process remains unclear in the literature. For example, rutile phase was proposed by Kim and Khalil, Khalil and Boccaccini [10,11]. According to the authors, when low amounts of TiO_2 (under 8 mol%) in SiO_2-based ceramic were chosen, sintering temperature decreases from 950 °C to 860 °C due to the introduction of [TiO_4] units into the silica network which would lead to the weakening of the chemical bonds. Several authors [12–16] studied the SiO_2–TiO_2 system and contradictory results emerge on the existence of solid solutions between silica and titania. In the literature, it is often suggested that a negligibly small content of titania (<5 wt%) in the silica-based solid solution would exist [12]. Four studies [13–16] report the existence of solid solutions. Ricker and Hummel [13] showed the presence of titania in α- and β-cristobalite and a solid solution of silica in rutile. In the same way, Evans [15] found a solid solution of TiO_2 in SiO_2 when the titania content ranges between 0 and 10.8 wt%. Finally, Nikitina [16] showed the existence of a SiO_2 (quartz)–TiO_2 solid solution for a TiO_2 content ranges up to 7.4 wt%.

To promote the formation of a liquid phase, bismuth oxide could also be considered as efficient sintering additive of silica-based ceramics. Indeed, in the SiO_2–Bi_2O_3 binary phase diagram, a liquid phase appears when the temperature of the peritectic invariant is reached:

$$\text{Liq} + SiO_{2(s)} \leftrightarrow Bi_4Si_3O_{12(s)} \text{ (silica content} \approx 60 \text{ mol\%) [17]} \quad (1)$$

Also, an eutectic at 740 °C could be observed in the Bi_2O_3–ZnO binary phase diagram for 85 mol% of Bi_2O_3 and 15 mol% of ZnO. The addition of a small quantity of $[Bi_2O_3\text{–ZnO}]_{eutectic}$ could lower the formation of the liquid phase. Last, the SiO_2–Bi_2O_3–ZnO ternary phase diagram reported in Fig. 1 [18] confirms the presence of an eutectic at 925 °C for the following composition: 26.97 wt% SiO_2 + 63.25 wt% Bi_2O_3 + 9.77 wt% ZnO.

According to literature, the use of both nanosized silica powders and additives such as titania or Bi_2O_3–ZnO eutectic compositions should be promising to enhance the densification kinetics of silica-based materials. The aim of the present article is twofold: firstly to determine the effect of these additives on the crystallization phenomenon of amorphous silica-based materials. This was done by using an original *in situ* characterization approach of the microstructural evolution. The second point is to investigate the interactions between the crystallization of materials and the densification kinetics as a function of the chemical composition of sintering additives. The three studied compositions are silica, SiO_2 + 15 wt% TiO_2, SiO_2 + 10 wt% $[Bi_2O_3\text{–ZnO}]_{eutectic}$, respectively.

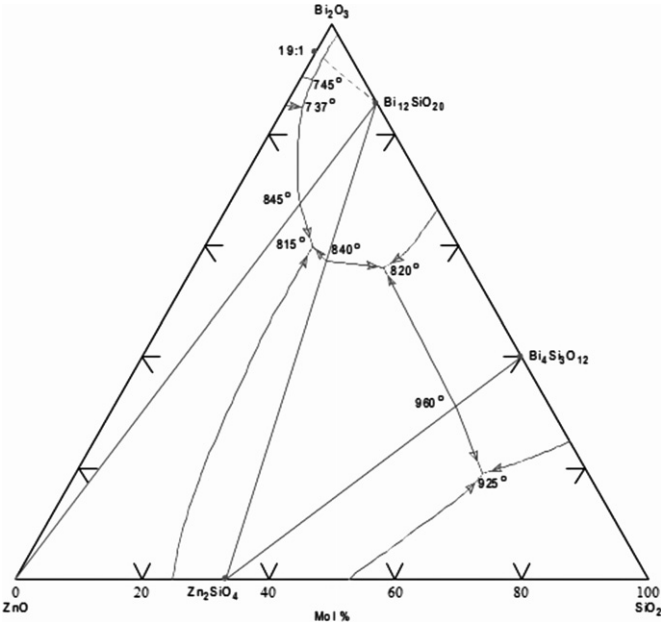

Fig. 1. Projections of liquidus layers in the SiO_2–Bi_2O_3–ZnO ternary phase diagram [18].

2. Experimental procedure

2.1. Raw materials

The mixture between the different primary oxides (SiO_2, TiO_2, ZnO) has been achieved with the help of colloidal suspensions. These precursors are commercial colloidal suspensions: amorphous silica (Aldrich Ludox AS-40, 99%, $\phi_m \approx 20$–24 nm, $S_{BET} \approx 135$ m^2/g with a concentration of 40 wt% in water, containing Na_2O from the dispersant used in the suspension (ratio $SiO_2/Na_2O = 192$)) later noted "silica", titania rutile (Nanoamor, 99.5%, $\phi_m \approx 30$–50 nm, $S_{BET} \approx 50$ m^2/g with a concentration of 40 wt% in water) and ZnO (NanoShield, +99.9%, $\phi_m \approx 70$ nm, $S_{BET} = 18$ m^2/g with a concentration of 50 wt% in water). In parallel, a Bi_2O_3 suspension has been prepared from a bismuth oxide powder (Alfa Aesar, +99.5%, $\phi_m \approx 38$ nm, $S_{BET} = 19$ m^2/g) and ammonium oleate as dispersant.

In order to reach a good chemical homogeneity of the mixtures, the SiO_2, Bi_2O_3, ZnO and TiO_2 aqueous suspensions were mixed in the following proportions: 85 wt% SiO_2 with 15 wt% of TiO_2 and 90 wt% of SiO_2 with 10 wt% of Bi_2O_3–ZnO eutectic (*i.e.* 85 mol% Bi_2O_3 + 15 mol% ZnO). The suspensions were mixed in aqueous medium to elaborate concentrated slurry of 20 vol%.

2.2. Shaping and sintering protocols

These mixed suspensions were evaporated in a rotary evaporator. The powder so-obtained was then dried and milled in an agate mortar. The powder was pelletized, *i.e.* the binder (3–50 wt% of (2/3PVA + 1/3 polyethylene glycol (PEG)) was pulverized on the powder, placed in a rotary bowl, to form granules which are dried and milled. The powder was uniaxially pressed (under a pressure of 200 MPa and using a 6 mm diameter die) to produce cylindrical pellets. The green body was 6 mm of diameter and 3 mm of thickness with a green relative density of $55 \pm 3\%$. Then, the samples were pre-heated at 400 °C at a heating rate of 1 °C/min and kept at that temperature for 16 h to burn out organic binders.

Sintering experiments were performed in air at a heating rate of 5 °C/min at 1400 °C.

2.3. Characterization techniques

Powder X-ray diffraction was performed using a Bruker D8 Advance (Champs-sur-Marne, France) diffractometer with a Cu($K\alpha_1$) source ($\lambda = 1.54056$ Å) in the Bragg Brentano $\theta - 2\theta$ geometry. The high-temperature X-ray diffractograms were recorded using a HTK 1200 N temperature cell (Anton Parr) equipped with a Lynxeye linear detector and a kapton–aluminum window foils. The temperature is limited to 1200 °C. The X-ray diffractograms were recorded with a 100 °C or 20 °C step from room temperature to 1000 °C. Samples were heated with a 5 °C/min heating rate and each recording lasts 1 h dwell time. The scans were performed from 15–90° in 2θ, with a step size of 0.016°/s.

The weight changes and the phase transformations (Tg, T_C) were indexed by using DTA and TGA coupled analyses (Netzsch evolution STA 409C, Selb, Germany). These experiments were carried out on green pellets up to 1200 °C with a 5 °C/min heating rate.

The geometrical variations of pellets during sintering have been measured by dilatometry up to 1400 °C with a heating rate of 5 °C/min and a dwell time of 3 h (Setaram TMA 92, Caluire, France).

The *in situ* microstructural evolution of compacts during sintering has been investigated using an environmental scanning electron microscope (Quanta 200 ESEM FEG, FEI Eindhoven, The Netherlands) equipped with a high temperature furnace. This specific apparatus has been described in details in reference [19]. These experiments have been carried out on pieces of pellets of millimeter size, with a heating rate of 30 °C/min from room temperature up to 900 °C and of 5 °C/min up to 1100 °C. The sample temperature is measured using a homemade crucible equipped with an inner Pt-PtRh10 thermocouple. All the experiments have been performed under a 250 Pa air atmosphere. Wavelength Dispersive Spectrometry (WDS) analyses on sintered pellets (after a treatment at 950 °C during 3 h) were obtained with a Castaing microprobe (Cameca SX100, Gennevilliers, France).

3. Thermal behavior of starting powders

Thermal analyses (TGA and DTA) under flowing air using a 5 °C/min heating rate were achieved in order to identify the sequence of phase transformations occurring for the present silica-based materials.

3.1. Silica

In the case of silica, the characteristic thermogram can be decomposed in three main parts (see Fig. 2a):

i) For temperatures ranging from 50 °C to 200 °C, the departure of the physisorbed water is responsible for

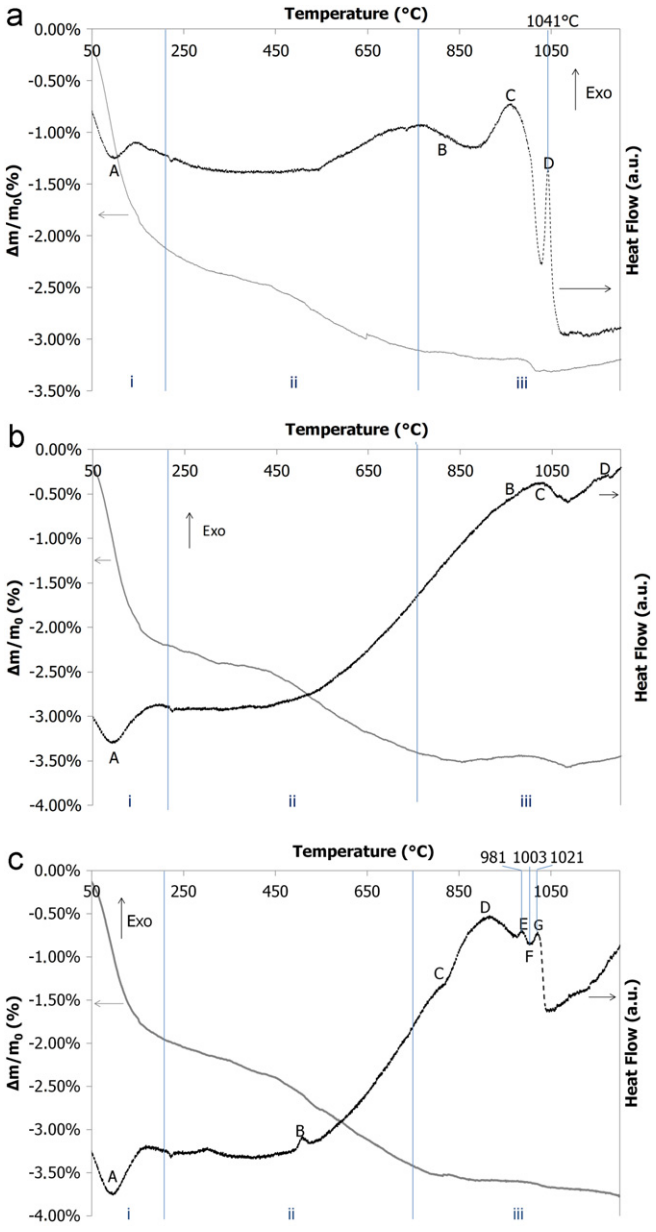

Fig. 2. Thermogravimetric (TGA) and differential thermal analyses (DTA) of (a) silica; (b) silica doped with TiO_2; (c) silica doped with $[Bi_2O_3–ZnO]_{eutectic}$ (heating rate ≈ 5 °C min^{-1}).

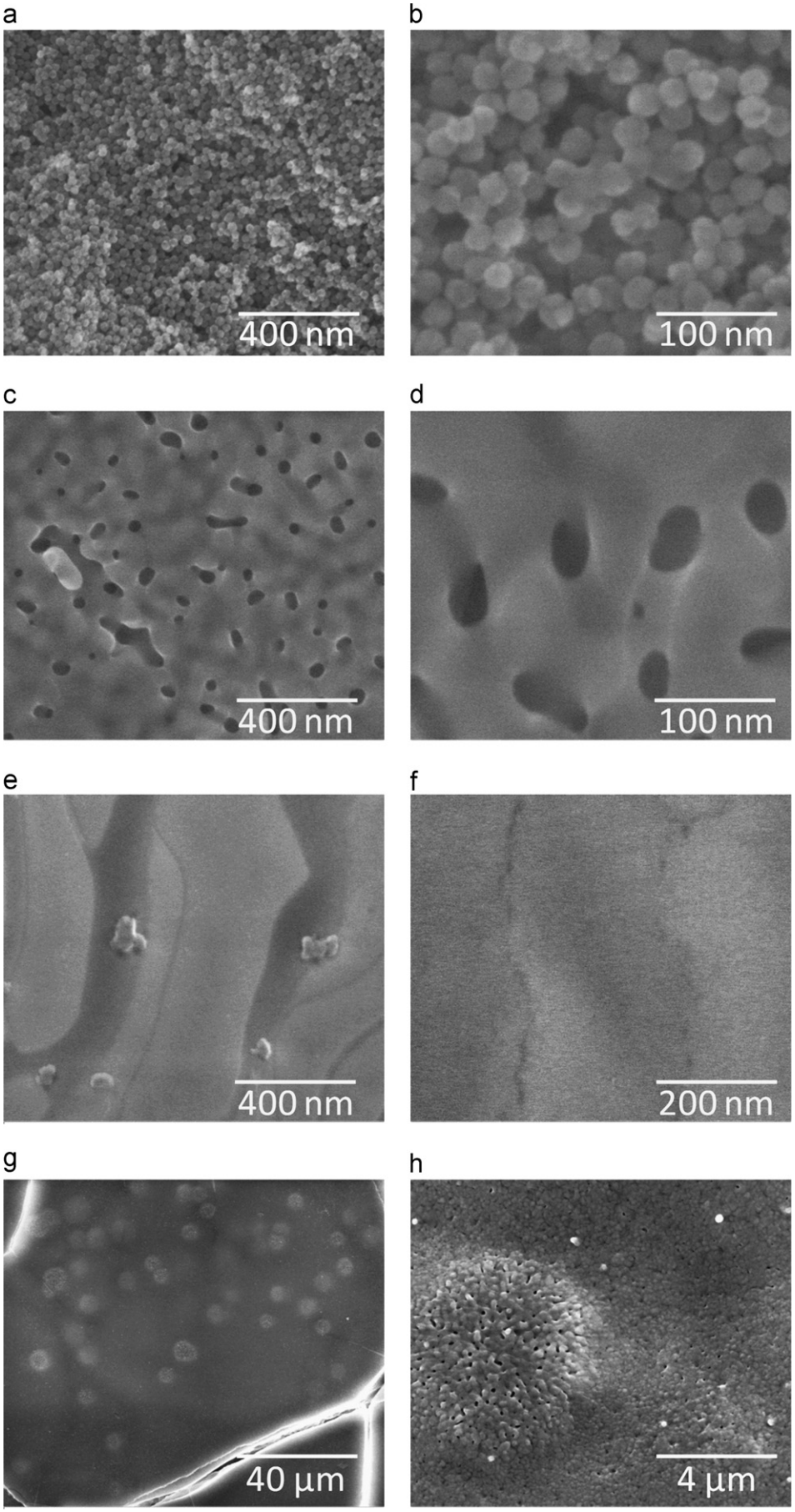

Fig. 3. ESEM micrographs of the surface of silica monoliths sintered at 500 °C (a), (b); 850 °C (c), (d); 950 °C (e), (f) and 1100 °C (g), (h).

the mass variation (loss of $\approx 2\%$) and is correlated to the (A) endothermic peak. In this temperature range, the surface is made out of terminal silanol groups (Si–OH) and siloxane bridges (Si–O–Si);

ii) Two successive phenomena lead to a weight loss of around 1% between 200 °C and 750 °C: (a) the removal of the organic auxiliaries (*i.e.*: PVA + PEG) when the temperature ranges between 200 °C and 400 °C ; (b) the condensation of strained silanol groups to form siloxane between 400 °C and 750 °C according to the Eq. (2) [5]:

$$\equiv Si-OH + HO-Si\equiv \rightarrow \equiv Si-O-Si\equiv + \overrightarrow{H_2O} \quad (2)$$

iii) in the last region (750 °C → 1100 °C), the weight loss remains low ($\approx 0.10\%$). This weight variation could be attributed to an endothermic effect which is embodied by a decreasing slope (effect noted (B)) around 825 °C. This would be characteristic of a glass transition. Then, an exothermic broad peak between 930 °C and 980 °C (noted (C)) is characteristic of crystallite nucleations. Then, a drift of the baseline is observed associated to a slight weight loss ($\approx 0.10\%$). This could be due to the "Topological Short Range Order" (TSRO) structural relaxation which would cause the densification of the sample [20]. Last, an exothermic peak (≈ 1041 °C) (noted (D)) is detected which is related to silica crystallization.

These results are coupled with ESEM analyses which show the evolution of the surface morphology of silica-based monolith as a function of the sintering temperature (*cf.* Fig. 3 (a–h)). From these images, the nanosized grains can be easily observed for silica, at 500 °C (see Fig. 3(a,b)). The average grain size is around 30 nm. Indeed, the morphology of particles remains unchanged for any temperature below 800 °C. When combining the observed grain morphology variations with the DTA-TGA data, one can determine that the glass transition (B) appears around 825 °C (see Figs. 2(a), 3(c,d)). Above 800 °C, the surface melting of silica particles appears as shown by the ESEM micrographs. For any temperature higher than 850 °C (see Fig. 3(c–h)), the grains are hardly distinguishable. These observations must be related to the formation of a glass phase above 850 °C. Indeed, the presence of a glass leads to fill partially the pores; it is characterized by the drift of the base line of the DTA curve above 945 °C characteristic of the sample densification. Then, crystallization phenomenon could take place around 1041 °C (D) for silica powder. Finally, residual pores are still visible at 1100 °C (see Fig. 3h), as well as spherulitic crystalline and amorphous phases (see Fig. 4).

The silica glass transition temperature usually reported in the literature is 1200 °C [2,3]. In this study, the DTA results show that for a silica powder which comes from a colloidal suspension with a certain amount of –OH groups and Na_2O, the glass transition temperature is 825 °C. Consequently, the glass transition of a silicate glass could be affected by the presence of the former or the modifier element in glass network as well as by the hydroxyl content. In the literature [21], it has been noticed that the glass transition temperature for SiO_2-based specimens containing high hydroxyl content occurs at lower temperatures. On that subject, Brückner [22], Brinker and Scherer [23] studied the variation of the glass transition temperature for the amorphous silica as a function of the hydroxyl content. More particularly, Brinker and Scherer [23] showed that the glass transition temperature should decrease when high –OH contents are reached because of the viscosity decrease. Brückner [24] has determined that the viscosity varies from 1.4 to 1.7 P for –OH content ranging from 3 to 1200 ppm and the activation energy varies from 510 to 711 kJ/mol. According to the literature [25], this activation energy corresponds to the α-relaxation transformation which is achieved by long-range cooperative motions of the atoms governed by viscous flow. The impurities (as –OH groups) cut the Si–O–Si bonds in the SiO_4 network which weakens the glass structure and reduces the viscosity.

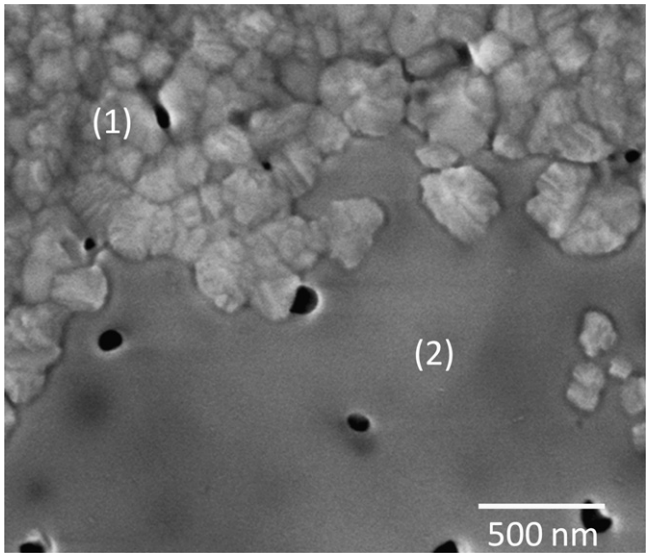

Fig. 4. ESEM micrograph of the surface of a silica sample sintered at 1100 °C with a crystalline zone (1) and an amorphous zone (2).

The X-ray diffractograms recorded on silica as a function of the sintering temperature are reported in Fig. 5(a). These diffractograms clearly show that the silica powder remains amorphous for any temperature lower than 940 °C. When the temperature becomes higher than 960 °C, the only crystallized phase that is detected is the cubic cristobalite phase. This phase is characterized by wide diffraction peaks due to the presence of ultrafine crystallites. These results are in good agreement with DTA and SEM data.

3.2. Doped-silica materials

When titania is used as an additive, similar thermal phenomena can be observed in comparison with those identified for silica (*cf.* Fig. 2b). Nevertheless, in the (ii)

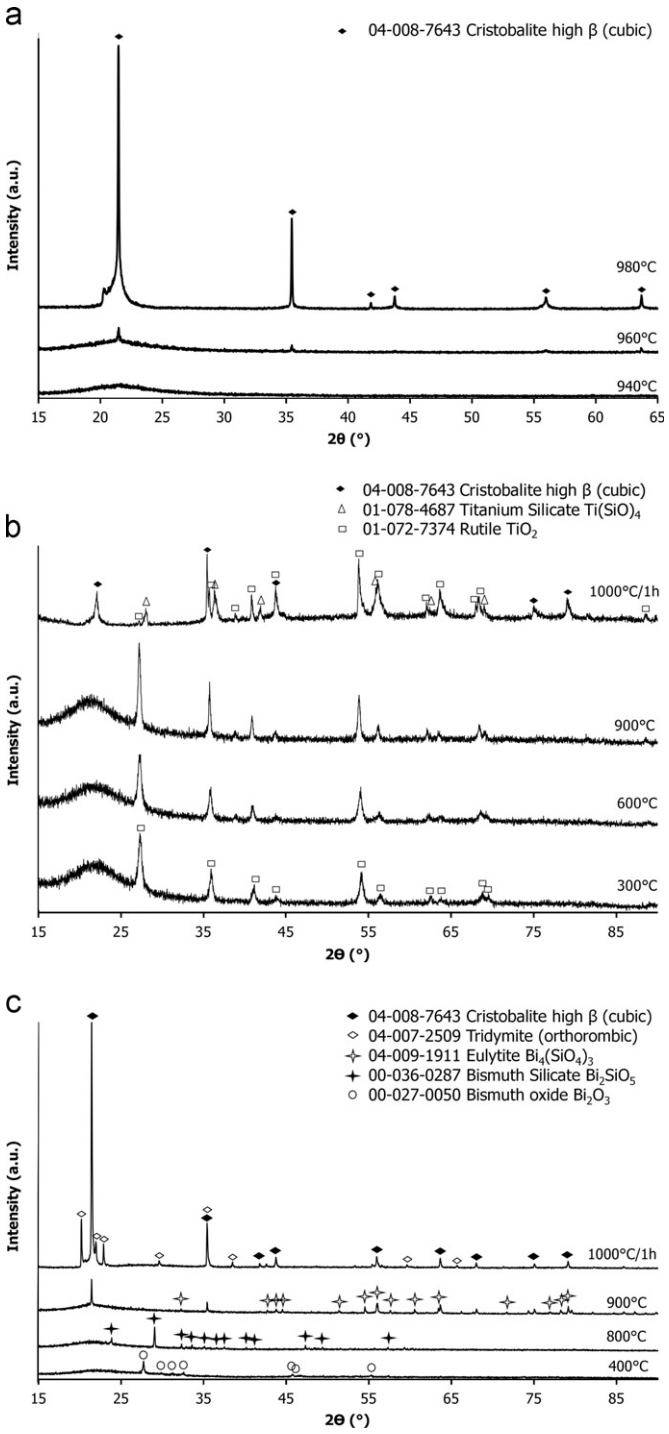

Fig. 5. XRD patterns at different temperatures for (a) silica; (b) silica doped with TiO_2; (c) silica doped with $[Bi_2O_3–ZnO]_{eutectic}$.

region, the condensation of both silanol groups and $Ti(OH)_4$ groups arises according to

$$Ti(OH)_4 \rightarrow TiO_2 + 2\,\overrightarrow{H_2O} \quad (3)$$

The weight loss associated to these condensation phenomena is of $\approx 1.40\%$, slightly higher than the weight loss in the same region for silica.

Then, in the (iii) region, there is no weight loss and the glass transition is expected to occur around 935 °C (B). The glass transition for silica doped with titania composition is less visible on the DTA curve than the glass transition observed on the DTA curve of silica. An exothermic broad peak between 980 °C and 1040 °C could be attributed to the nucleation (C). A weak exothermic peak could be inferred at 1132 °C (D), corresponding to the crystallization temperature.

ESEM micrographs (Fig. 6 (a–h)) show that titania-doped silica based materials react differently in comparison with silica. Silica grains are still present up to 950 °C (see Fig. 6 (c,d)) when titania is added and for any temperature higher than 950 °C a glass seems to be formed.

In the case of $[Bi_2O_3–ZnO]_{eutectic}$ additive (see Fig. 2c), several thermal phenomena can be successively identified. In particular, in the ii) region, an exothermic peak is noticeable at 507 °C (B) which could be due to the Bi_2SiO_5 crystallization. The weight loss in this region is 1.75% due to the silanol groups condensation. In the iii) region the weight loss is around 0.25%. This loss might be related to the slight volatilization of Bi_2O_3 above 810 °C. A glass transition (C) is expected to occur around 800 °C, followed by the nucleation (D) and a crystallization effect (E) that takes place at 981 °C. This result coupled with the XRD diffractograms (see Fig. 5c) at 1000 °C can be associated to the cristobalite phase crystallization. The melting of eulytite (F) at 1003 °C [26] and the crystallization of tridimyte at 1021 °C (G) are observed. The measured melting temperature is higher than that expected ($T=740$ °C). This effect could be attributed to the partial volatilization of Bi_2O_3 during the heating which leads to a small deviation from the targeted composition. The WDS analyses indicate that only 7 wt% Bi_2O_3 remain in the samples that have been sintered at 950 °C for 3 h, while 9.7 wt% Bi_2O_3 have been initially introduced in the reactive mixtures. This confirms the partial volatilization of bismuth oxide ($\approx$ 3 wt%).

The X-ray diffractograms recorded in temperature for silica doped with TiO_2 and with $[Bi_2O_3\text{-}ZnO]_{eutectic}$ are reported in Fig. 5(b, c), respectively. For TiO_2-doped silica, characteristic peaks of a titanium-silicate ($Ti(SiO)_4$) and cubic cristobalite begin to appear on the HT-XRD recorded at 1000 °C. In the case of silica doped by $[Bi_2O_3–ZnO]_{eutectic}$, Bi_2O_3 reacts preferentially with silica by forming successively Bi_2SiO_5 before 800 °C and $Bi_4(SiO_4)_3$ (eulytite) at 900 °C as expected by the corresponding phase diagram (see Fig. 1).

The main reactions which occur during heat treatment for different compositions (silica, SiO_2+TiO_2 and $SiO_2+[Bi_2O_3–ZnO]_{eutectic}$) are summarized in Table 1.

4. Sintering behavior

The relative shrinkage (Fig. 7a) and the corresponding derivate curves (see Fig. 7b) of the different compositions have been determined up to 1400 °C.

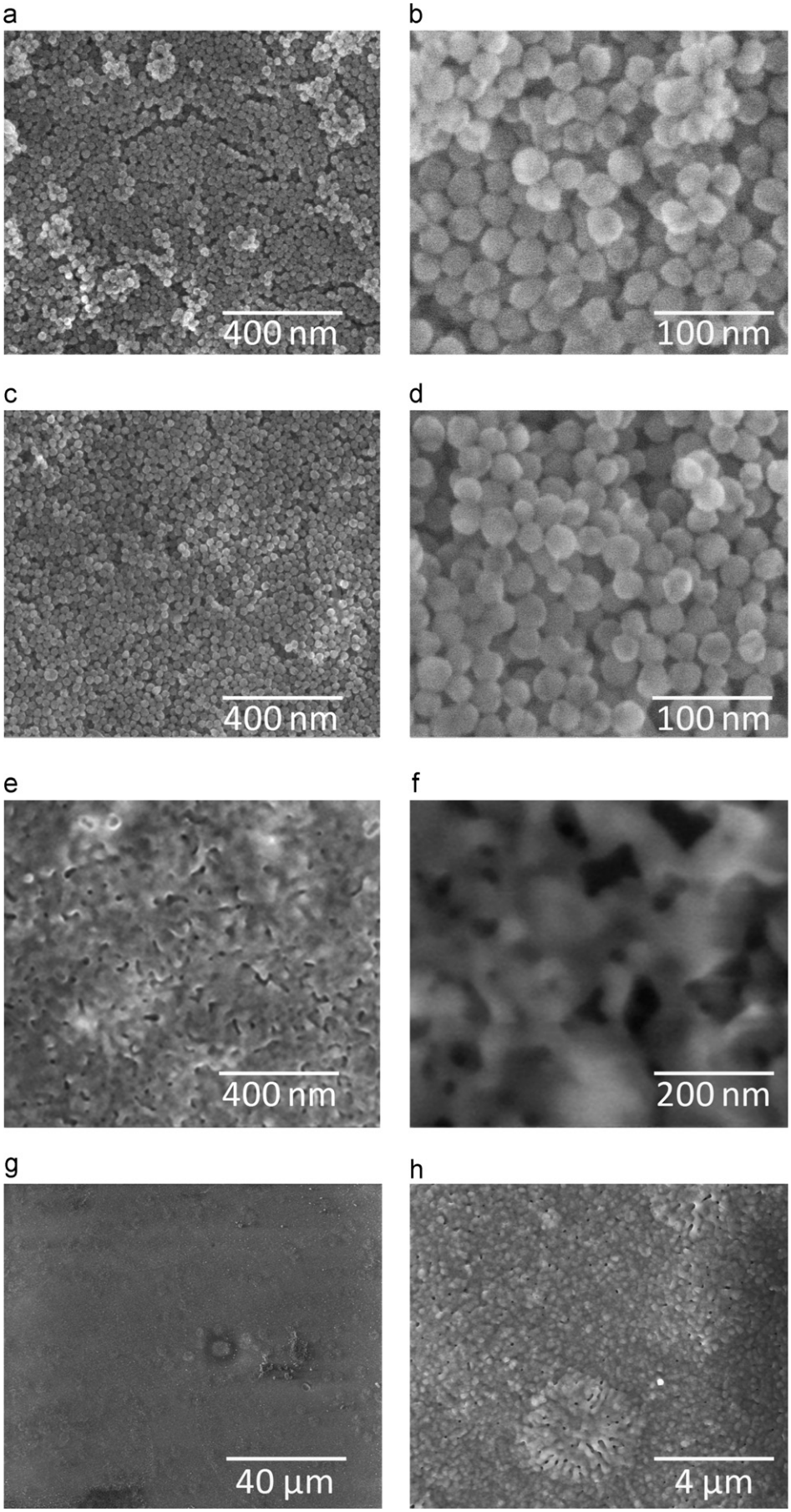

Fig. 6. ESEM micrographs of the surface of SiO_2–TiO_2 monoliths sintered at 500 °C (a), (b); 850 °C (c), (d); 950 °C (e), (f) and 1100 °C (g), (h).

Table 1
Sequence of sintering reactions occurring during the heat treatment of SiO_2, SiO_2+TiO_2 and $SiO_2+[Bi_2O_3–ZnO]_{eutectic}$.

Transformation	(i)	(ii)		(iii)				
Silica	$T<200$ °C	200 °C $<T<$ 400 °C	400 °C $<T<$ 700 °C	825 °C	930–980 °C	1041 °C		
	Removing of physisorbed water	Removing of organic auxiliary	Condensation of silanol groups to form siloxane	Glass transition	Nucleation	Crystallization of silica in cristobalite		
SiO_2+TiO_2	Removing of physisorbed water	Removing of organic auxiliary	400 °C $<T<$ 800 °C	935 °C	980–1040 °C	1132 °C		
			Condensation of both silanols groups and $Ti(OH)_4$ groups	Glass transition	Nucleation	Crystallization of silica in cristobalite		
$SiO_2+[Bi_2O_3$-$ZnO]_{eutectic}$	Removing of physisorbed water	Removing of organic auxiliary	507 °C Crystallization of Bi_2SiO_5	800 °C Glass transition	880-930 °C Nucleation	981 °C Crystallization of silica in cristobalite	1003 °C Eulytite melt	1021 °C Crystallization of silica in tridymite

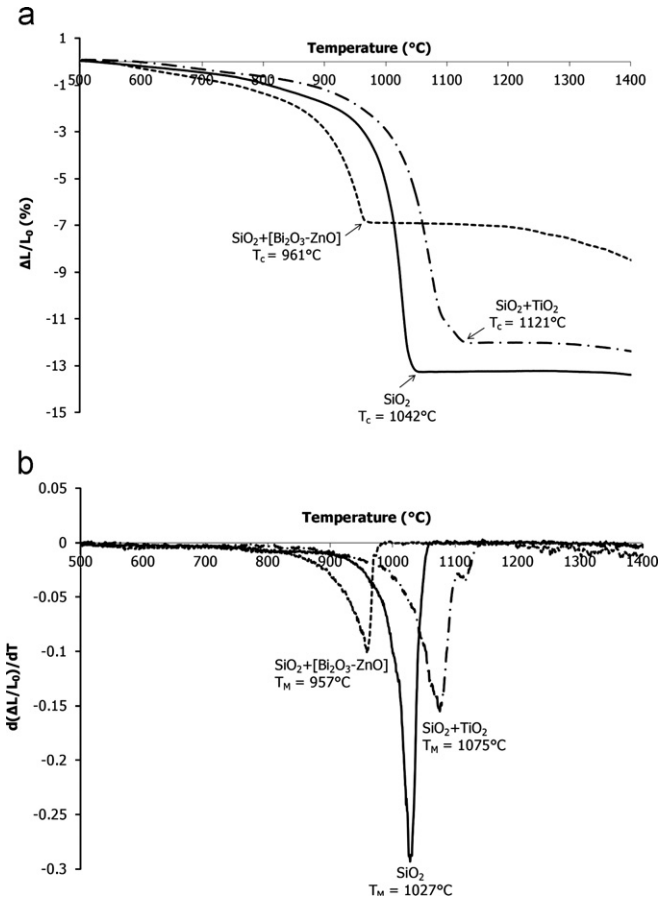

Fig. 7. (a) Relative shrinkage of silica, SiO_2–TiO_2, $SiO_2+[Bi_2O_3–ZnO]_{eutectic}$ and (b) corresponding derivative curve during heating.

4.1. Anisothermal conditions

The densification curve of silica (Fig. 7a) can be divided as a function of the temperature in three parts. At low temperature, the sintering of amorphous silica takes place: the relative shrinkage increases with increasing temperature due to the decrease of the viscosity of amorphous phase ($T<1100$ °C). The temperature of the maximum of the densification rate (T_M) is observed at 1027 °C (see Fig. 7b). The second part of the curve corresponds to the plateau: the shrinkage becomes inhibited due to the crystallization of amorphous silica into cristobalite. The temperature for the densification inhibition (1042 °C) corresponds to the crystallization temperature identified by DTA analyses (1041 °C) (see Fig. 2a). At higher temperature, a second shrinkage is observed due to the sintering of the cristobalite phase ($T>1300$ °C).

In the same way, the dilatometric derivate curve recorded on a $SiO_2+10\%$ $[Bi_2O_3–ZnO]_{eutectic}$ additive is reported on Fig. 7b. The obtained data indicates that the introduction of $[Bi_2O_3–ZnO]_{eutectic}$ additive decreases the temperature of the maximum densification rate (T_M) to 957 °C, *i.e.* 70 °C lower than the determined value for silica.

Additions of titania has the opposite effect since this characteristic temperature (T_M) is increased (*i.e.* 1075 °C). Kim and Khalil [10], Khalil and Boccaccini [11] have measured lower sintering temperatures, varying from 950 °C to 860 °C when TiO_2 content ranges from 0 to 8 mol%, respectively. According to these authors [10,11], the addition of TiO_2 into the silica glass yields to a decrease of its viscosity. Indeed, the substitution of Si^{4+} by Ti^{4+} would soften the silica glass network. Nevertheless, in the present study, the addition of TiO_2 does not reduce both the sintering and the crystallization temperatures when compared to silica. This discrepancy could be explained by the decreasing of the reactivity between SiO_2 and TiO_2 either because the dispersion of SiO_2 and TiO_2 nanopowders in a compact is less homogeneous than in gels even if the WDS analyses do not exhibit compositional heterogeneities or because the sintering temperature of silica nanopowders is lower than the substitution temperature of titania into silica network for nanopowders.

Nevertheless, for both cases, when $[Bi_2O_3–ZnO]_{eutectic}$ or TiO_2 are added, the densification rate is lower than that determined for silica. The crystallization temperature can be determined as the temperature for which the first step of

densification is roughly switched off (see Table 2). This temperature shift between the two data sets can be attributed to the location of the thermocouples in the furnaces: in the DTA equipment, the thermocouple is localized near the sample whereas in the dilatometric equipment it is directly in contact with the sample. The crystallization temperatures determined from HT-ESEM movies are of the same order of magnitude (see Table 2).

To identify accurately the phase transition and the subsequent microstructural evolution for the three compositions of silica-based materials, *in situ* high temperature environmental scanning electron microscope (HT-ESEM) experiments have been carried out. The image series are turned into videos (see video 1 [27]). Characteristic micrographs of the microstructural transformation occurring in these conditions have been reported in Fig. 8 for $SiO_2+[Bi_2O_3–ZnO]_{eutectic}$ composition. No modification of the sample microstructure is observed until 967 °C. Then, sudden changes of microstructure appear. Propagation fronts arise and move fast through the specimens (see Fig. 8 or video 1 [27]). It can be noticed that the beginning temperature of the drastic microstructure changes corresponds to the crystallization temperature determined by DTA and dilatometric analyses.

The values of the speed of the crystallization front, issued from the ESEM micrographs, have been reported in Table 2. It could be noticed that the speeds of crystallization fronts have been determined at the maximum crystallization temperatures for each studied system. The speed of the crystallization front appears to be fastened by the addition of $[Bi_2O_3–ZnO]_{eutectic}$ to silica, while it is lowered when TiO_2 is added to silica. Similar studies have been carried out on amorphous silica under H_2O, dry air, N_2, O_2 or vacuum atmospheres for temperatures above 1300 °C [22], [28–30]. Speeds of crystallization fronts have already been determined by Brückner [22] for silica in a 478 mm water vapor pressure atmosphere at 1460 °C. The obtained value is 1.6×10^{-8} m/s. This value is lower than the one determined in the present study for silica in air at $T=1070$ °C, *i.e.* 400 °C lower. The presence of Na_2O in the silica precursor used in this study could explain this difference. Indeed, Brückner [22] has shown that the addition of 0.32 wt% Na_2O to silica yielded to an increase of the speed of the crystallization front up to 1.2×10^{-5} m/s at $T=1400$ °C.

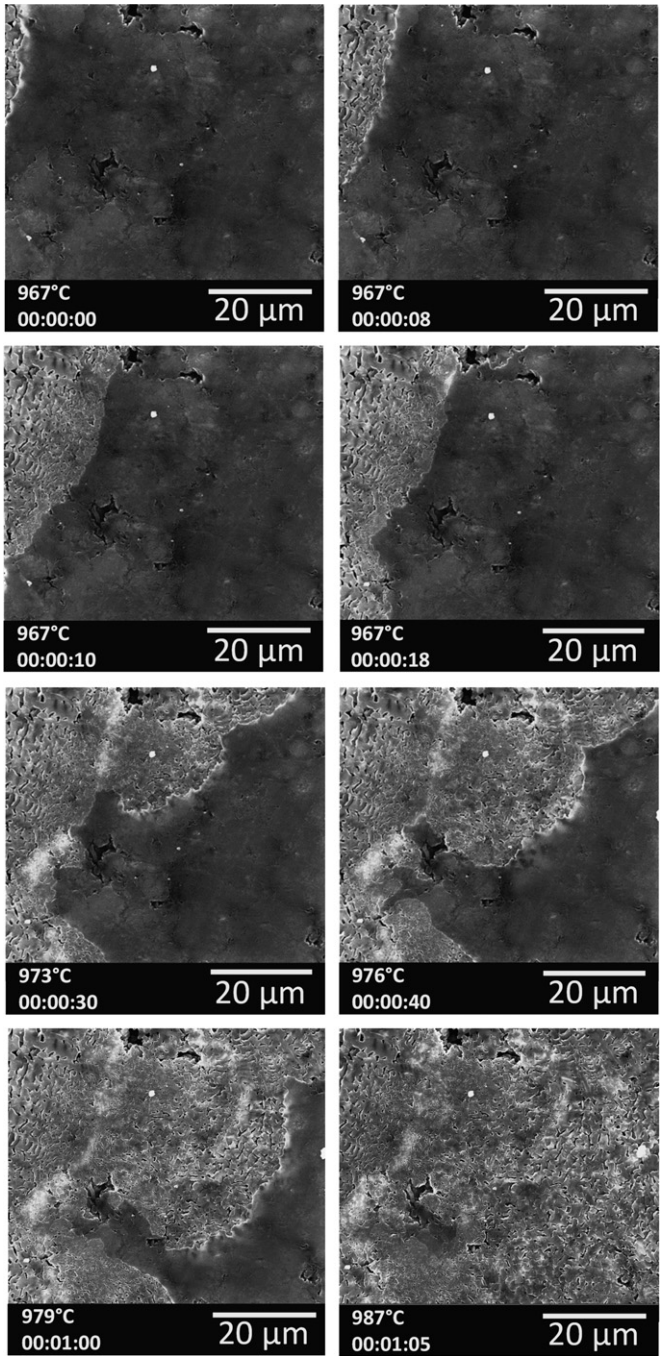

Fig. 8. HT-ESEM micrographs for silica doped with $[Bi_2O_3–ZnO]_{eutectic}$.

Table 2
Data collection of the characteristic values determined in this work as a function of the studied system.

Studied effect	Studied system	SiO_2	SiO_2+TiO_2	$SiO_2+[Bi_2O_3–ZnO]$
Sintering	T_M (Dilatometry) (°C)	1027 ± 8	1075 ± 8	957 ± 8
Crystallization	T_C (Dilatometry) (°C)	1042 ± 8	1121 ± 8	961 ± 8
	T_C (DTA) (°C)	1041 ± 2	1132 ± 2	981 ± 2
	T_C (HT-ESEM) (°C)	1080 ± 30	1120 ± 30	980 ± 30
Average speed of crystallization fronts determined at the crystallization temperature ($m\,s^{-1}$)		4×10^{-7}	8×10^{-8}	1×10^{-6}

The effect of additional elements to silica used in this study could be summarized as follows: when Bi_2O_3 and ZnO are added to silica, they act as glass former species. This means that it leads to a viscous flow at lower temperatures. The viscous flow yields to a granular rearrangement during the first stage of the sintering leading to the densification of the sample. This explains the decrease of the sintering temperature measured at 957 °C for the $SiO_2+[Bi_2O_3+ZnO]_{eutectic}$ composition compared to 1027 °C for silica. The effect of the addition of TiO_2 to silica is opposite as it is an intermediate oxide, which role depends on the glass composition. In the present case, the TiO_2 addition is accompanied by the decrease of the speed of the crystallization front, which can be associated to a stiffening of the silica structure.

4.2. Effect of crystallization on the sintering of amorphous silica

From the previous experimental results, it clearly appears that the crystallization phenomenon occurs after the glass transition.

One sample of each composition has been heat treated at 1200 °C, *i.e.* at higher temperature than the crystallization temperature. Some characteristic SEM micrographs have been reported in Fig. 9. For temperatures higher than the crystallization temperatures, the microstructure is characterized by the presence of many pores with various shapes and sizes (from 100 nm to 10 μm). The presence of a high amount of pores is related to the crystallization process. For the $SiO_2+[Bi_2O_3–ZnO]_{eutectic}$ composition, two zones can be observed: a vitreous matrix mainly composed of silica (gray zone) and some crystals which are constituted of silicon, bismuth and oxygen. These elementary chemical analyses coupled with XRD results suggest that these crystals obey to the $Bi_4Si_3O_{12}$ composition. The observation of this phase indicates that the crystallization of the $SiO_2+[Bi_2O_3–ZnO]_{eutectic}$ composition is accompanied by both the formation of well-defined compounds and the conversion of silica vitreous phase into cristobalite and tridymite phases.

The crystallization process induces coarse pores that cannot be removed during the sintering even if the temperature is higher than the sintering or crystallization ones. This microstructure is observed in the crystallized zone of the HT-ESEM images (see Fig. 8 or video 1 [27]). Scherer [31] explain that the crystallization effect on sintering depends on the position of the nucleation sites and on their growth rate.

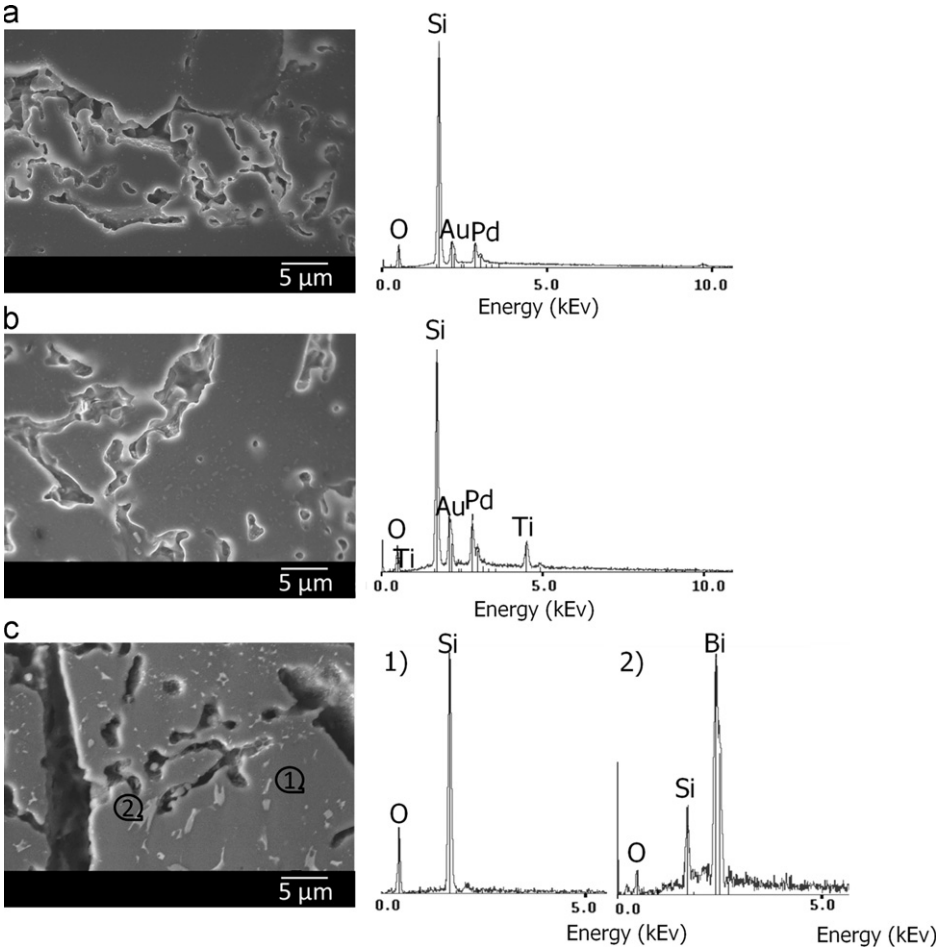

Fig. 9. SEM images and EDXS analyses for silica (a), $SiO_2–TiO_2$ (b), $SiO_2+[Bi_2O_3–ZnO]_{eutectic}$ (c) after sintering at 1200 °C.

In the present case, the crystallization remains sufficiently fast to inhibit the densification process before reaching the later stages of sintering. Thus, for each composition, a huge amount of pores is trapped within the crystalline zone and the achievement of full density is severely limited, even after prolonged heat treatment at high temperature. As a consequence, the second part of the dilatometric curve (*i.e.* when the temperature is higher than the crystallization temperature), corresponding to the cristobalite densification, can be associated to the surface modifications (observed after crystallization on video 1 [27]). The removing of the trapped porosity remains very slow and this does not lead to the complete densification of the sample. The sintering of silica is a viscous sintering, and the nucleation of nano-crystals forms obstacles for viscous flow motion, leading to a viscosity increase and consequently to an inhibition of the densification [31].

5. Conclusions and perspectives

The low temperature silica sintering has been investigated regarding the effect of 10 wt% $[Bi_2O_3–ZnO]_{eutectic}$ and 15 wt% TiO_2 additions to silica.

The obtained results clearly show that the sintering and crystallization temperatures of silica are lowered by 70 to 80 °C by adding 10 wt%[Bi_2O_3-ZnO] and are increased by 50 °C to 80 °C when TiO_2 is added.

The crystallization takes place after the glass transition. The speed of the crystallization fronts have been measured for the three compositions, using HT-ESEM image series. In the case of silica, the speed of crystallization front determined at the crystallization temperature ($T=1080$ °C) is 4×10^{-7} m/s. The additives that have been studied have opposite effects on crystallization kinetics of silica: the first one, TiO_2 leads to a lower speed of crystallization front at 1120 °C (*i.e.* 8×10^{-8} m/s), whereas the second one, $[Bi_2O_3–ZnO]_{eutectic}$ leads to a higher speed of crystallization front at 980 °C (*i.e.* 1.10^{-6} m/s).

As the sintering of silica-based materials obeys to a viscous flow assisted mechanism, the densification is then drastically inhibited by the formation of crystals which rapidly damps the viscous flow motion.

In the field of microelectronic applications, where silica could potentially be used in combination with silver, the decrease of the sintering temperature of silica - as established in this work using silica nanopowder—could be very promising. However, the sintering kinetics of doped-silica and silver are over different to avoid the appearance of microcracks at the metal/ceramic interface. To fit the shrinkage kinetics during the sintering treatment, silver can be doped with palladium, platinum or with a small amount of silica that will not degrade the conductive properties of silver.

Acknowledgments

This work was financially supported by the DGA, the Limousin Council, Elopsys and the European Center of Ceramic in the framework of the CermJet program (*i.e.* of the 7th call of FUI Research Program).

References

[1] R.C. Buchanan, Ceramic Materials for Electronics, Third Edition, CRC Press, Ohio, the United States, 2004.
[2] J. Barton, C. Guillemet, Le verre: Science et technologie, EDP Sciences, Les Ulis, France, 2005.
[3] K.-D. Kim, G. Ondracek, Phase diagrams and sinter aids (Cs_2O) for SiO_2-sinterglass, Journal of Materials Science Letters 13 (2) (1994) 89–90.
[4] S.-W. Wu, D.S.H. Wong, S.-Y. Lu, Size effects on silica polymorphism, Journal of the American Ceramic Society 85 (10) (2002) 2590–2592.
[5] R.L.W. Popma, Sintering characteristics of nano-ceramic coatings, Ph.D. Thesis, University Library Groningen, Groningen, The Netherlands (2002).
[6] T.J. Rockett, W.R. Foster, Phase relations in the system boron oxide–silica, Journal of the American Ceramic Society 48 (2) (1965) 75–80.
[7] S. Wang, H. Zhou, Densification and dielectric properties of CaO–B_2O_3–SiO_2 system glass ceramics, Materials Science and Engineering: B 99 (1–3) (2003) 597–600.
[8] H. Shao, T. Wang, Q. Zhang, Preparation and properties of CaO–SiO_2–B_2O_3 glass-ceramic at low temperature, Journal of Alloys and Compounds 484 (1–2) (2009) 2–5.
[9] H. Zhu, H. Zhou, M. Liu, P. Wei, G. Ning, Low temperature sintering and properties of CaO–B_2O_3–SiO_2 system glass ceramics for LTCC applications, Journal of Alloys and Compounds 482 (1–2) (2009) 272–275.
[10] K.-D. Kim, T. Khalil, Sintering behavior of gel powder in binary glass-forming SiO_2–TiO_2 system, Journal of Non-Crystalline Solids 195 (3) (1996) 218–222.
[11] T.K. Khalil, A.R. Boccaccini, Heating microscopy study of the sintering behaviour of glass powder compacts in the binary system SiO_2–TiO_2, Materials Letters 56 (3) (2002) 317–321.
[12] R.C. De Vries, E.F. Osborn, The system SiO_2–TiO_2, Transaction British Ceramic Society 53 (9) (1954) 525–540.
[13] R.W. Ricker, F.A. Hummel, Reactions in the system TiO_2–SiO_2; revision of the phase diagram, Journal of the American Ceramic Society 34 (9) (1951) 271–279.
[14] R. Rieke, Melting influence of titanic acid on silica, alumina and kaolin, Sprechsaal 41 (1908) 405–406.
[15] D.L. Evans, Solid Solution of TiO_2 in SiO_2, Journal of the American Ceramic Society 53 (7) (1970) 418.
[16] I.P. Nikitina, Solid solutions in the system SiO_2–TiO_2, Neorganicheskie Materialy 11 (1975) 2094–2095.
[17] Y.T. Fei, S.J. Fan, R.Y. Sun, J.Y. Xu, M. Ishii, Crystallizing behavior of Bi_2O_3–SiO_2 system 19 (10) (2000) 893–895.
[18] V.M. Skorikov, P.F. Rza-Zade, Y.F. Kargin, F.F. Dzhalaladdinov, Equilibrium phases in the systems ZnO–Bi_2O_3–SiO_2 and ZnO–Bi_2O_3–GeO_2, Inorganic Chemistry 26 (7) (1981) 1026–1028.
[19] R. Podor, N. Clavier, J. Ravaux, L. Claparede, N. Dacheux, D. Bernache-Assollant, Dynamic aspects of cerium dioxide sintering: HT-ESEM study of grain growth and pore elimination, Journal of the European Ceramic Society 32 (2) (2012) 353–362.
[20] G.W. Koebrugge, J. Sietsma, A. van den Beukel, Structural relaxation and equilibrium free volume in amorphous $Pd_{40}Ni_{40}P_{20}$, Journal of Non-Crystalline Solids 117–118 (1990) 609–612.
[21] R.K. Iler, The Chemistry of Silica: Solubility, Polymerization, Colloid and Surface Properties and Biochemistry of Silica, Wiley-Interscience, California, the United States, 1979.
[22] R. Brückner, Properties and structure of vitreous silica I, Journal of Non-Crystalline Solids 5 (2) (1970) 123–175.

[23] C.J. Brinker, G.W. Scherer, Sol–Gel Science: The Physics and Chemistry of Sol–Gel Processing, Gulf Professional Publishing, California, the United States, 1990.
[24] R. Brückner, Properties and structure of vitreous silica II, Journal of Non-Crystalline Solids 5 (3) (1971) 177–216.
[25] K. Saito, N. Ogawa, A. Ikushima, Y. Tsurita, K. Yamahara, Effects of aluminum impurity on the structural relaxation in silica glass, Journal of Non-Crystalline Solids 270 (1–3) (2000) 60–65.
[26] Y.T. Fei, S.J. Fan, R.Y. Sun, M. Ishii, Study on phase diagram of Bi_2O_3–SiO_2 system for Bridgman growth of $Bi_4Si_3O_{12}$ single crystal, Progress in Crystal Growth and Characterization of Materials (2000) 183–188.
[27] L. Nguyen, A. Maître, M. Lejeune, C. Dossou-Yovo, R. Noguera, R. Podor, Video 1, 〈https://docs.google.com/open?id=0B31mihHM8ezLVlA2MlhidHJDcDA〉 (link verified on December 17th 2012).
[28] F.E. Wagstaff, K.J. Richards, Kinetics of crystallization of stoichiometric SiO_2 glass in H_2O atmospheres, Journal of the American Ceramic Society 49 (3) (1966) 118–121.
[29] F.E. Wagstaff, Crystallization kinetics of internally nucleated vitreous silica, Journal of the American Ceramic Society 51 (8) (1968) 449–453.
[30] F.E. Wagstaff, Crystallization and melting kinetics of cristobalite, Journal of the American Ceramic Society 52 (12) (1969) 650–654.
[31] G.W. Scherer, Effect of inclusions on shrinkage, in: B.J.J. Zelinski, C.J. Brinker, D.E. Clark, D.R. Ulrich (Eds.), Better Ceramics Through Chemistry VI, Materials Research Society, Pittsburh, Pennsylvania, 1990, pp. 503–514.